JOURNAL OF SEMICONDUCTOR TECHNOLOGY AND SCIENCE, VOL.12, NO.2, JUNE, 2012 http://dx.doi.org/10.5573/JSTS.2012.12.2.219

Implementation of Electrochemical Methods for Metrology and Analysis of Nano Electronic Structures of Deep Trench DRAM

Tadios Tesfu Zeru, Stephan Schroth, and Peter Kuecher

***Abstract*—In the course of feasibility study the necessity of implementing electrochemical methods as an inline metrology technique to characterize semiconductor nano structures for a Deep Trench Dynamic Random Access Memory (*DT-DRAM*) (e.g. ultra shallow junctions *USJ*) was discussed. Hereby, the state of the art semiconductor technology on the advantages and disadvantages of the most recently used analytical techniques for characterization of nano electronic devices are mentioned. Various electrochemical methods, their measure relationship and correlations to physical quantities are explained. The most important issue of this paper is to prove the novel usefulness of the electrochemical micro cell in the semiconductor industry.**

***Index Terms*—Ultra shallow junctions, DT-DRAM, electrochemical micro cell, nano electronic technology**

I. INTRODUCTION

The fundamental challenge for factory metrology is the implementation of new methods that measure material properties and control at atomic dimensions while maintaining profitable high volume manufacturing. Challenges in metrology of semiconductor nano structures can be found in both CMOS extension and beyond CMOS as suggested by ITRS. Some of these techniques have the ability to measure properties of materials such as thickness on the sidewalls of densely patterned features such as gates, FINS and the interfaces of deep trenches. Another unambiguous challenge is to find a nondestructive material characterization or imaging method that measures the material properties at atomic dimensions. Here, the most often mentioned goal is to provide 3D, atomic resolution measurements. The fact that some materials properties are not localized to atomic dimensions as reported by [1] is noteworthy.

Therefore the ongoing research focuses on finding a solution for the problems that from the tremendous down-scaling of the electronic structures of Deep Trench Dynamic Random Access Memory *(DT-DRAM)*. Researchers in the semiconductor industries and other research institutions are developing various novel ultra thin layer materials (e.g. high-*K*) that allow more packaging space and enhance the performance of transistors. Besides the positive effects of down-scaling mentioned above, there are some negative impacts which are a quantum mechanical phenomenon; such as unpredicted current leakage (tunneling effect). According to literature, the decreasing of lateral area of *DT-DRAMS* towards 10 nm scales will cause a devastating loss of energy due to the increase of static power (power consumed when no signal activity occurs). It is related to the size and configuration of the transistors [2], doping concentration and layer thickness fluctuation of semiconductors [3]. The doping fluctuation for a MOSFET doped with 10^{18} atoms per cm^3 corresponds to 4 atoms in 10 nm^3 [3]. The three major components which empower static power are:

Manuscript received Aug. 16, 2011; revised Jan. 19, 2012.
Dechema e.V., Theodor Heuss-Allee 25, D-60486 Frankfurt, Germany
E-mail : Tesfu@dechema.de, T.Tesfu@gmx.de

- Sub-threshold leakage from source to drain
- Gate leakage
- Reversed bias junction leakage

Gate leakage or the uncontrolled current flux of a gate when it is off can be avoided with materials having a higher dielectric constant and an improvement of capacitor performance can be achieved by increasing the aspect ratio of the deep trench capacitor. So we find it reasonable to implement an alternative way or method of precisely determining the layer thickness of gate oxides, the interface of *DT*-capacitors and the doping state of ultra shallow junctions (*USJ*). *USJ* are thin doping layers which are the most important part of a transistor. Hereby electrochemical impedance spectroscopy and cyclic voltammetry combined with an electrochemical micro cell are used to characterize doping type, doping concentration and the influence of annealing activation of *USJ*. Electrochemical methods are nondestructive opposed to e.g. ToF-SIMS which was primarily used to determine the doping concentration of semiconductor structures.

II. Review and Feasibility Discussion

1. Destructive technique

Recently in the semiconductor industries, secondary ion mass spectroscopy (*SIMS*), ellipsometry and *XRD* (X-ray diffraction) can be used to determine doping state, layer thickness and the material composition of a transistor. *SIMS* is a destructive analytical method, where the analysis occurs during the destruction of the sample or the material. This is not a preferable method for industrial inline analysis for the characterization of gate dielectrics or the composition of the capacitor of a transistor. A charge storage capacitor of *DT* technology is fabricated by etching high aspect ratio vertical trenches into a silicon substrate using thick silicon dioxide hardmasks. The bottom dimension is obtained by consequent resistor structuring of nitride, amorphous silicon and oxide hardmask opening steps. A direct measurement of this deep trench mask open bottom dimension allows both feed back control of the mask open etch process sequence and feed-forward control of the *DT* main etch [4]. There is a metrological challenge in analyzing the aspect ratio of the hard mask profile. Therefore a non destructive method is highly wanted.

2. Non destructive techniques

Yet there are three nondestructive analysis techniques such as firstly atom force microscopy (*AFM*), secondly a model based infrared reflectometry and third a visible light scatterometry used to characterize such structure depth profile, but with major limitations [4].

The first non destructive technique *AFM* is a direct depth measurement method at the current node [5]. For the future node *AFM* will have tip penetrating hindrances in the narrow recess (openings) of the deep trench capacitor.

Silicon is transparent in the infrared range. Therefore the results of the second non destructive technique, a model based infrared reflectometry, can be eliminated due to the employed wavelength between the range of 1 to 20 microns from back features of the specimen.

Therefore the third non destructive technique called Scatterometry can be used to determine critical dimensions of periodical structures on a pitch range smaller than 30 nm and dimension structures with high aspect ratio. However scatterometry is also sensitive to many other details of structure and therefore requires extensive modeling, which is time consuming for use as inline metrology [4].

3. Electrochemical methods

Electrochemical methods may be suggested alternatively as electrochemical impedance spectro-scopy (*EIS*), cyclic voltammetry (*CV*), relaxation voltammetry (*RV*) and four point probe (μ-4*PP*) resistivity measurements. These are neither vacuum requiring nor destructive; thus a specimen or material can be characterized accurately without any damage.

In the semiconductor industry a classical μ-4*PP* method as electrochemical characterization technique is used to analyze sheet resistance of source drain structures and ultra shallow junction (*USJ*) of gate dielectrics. The micro probe, with a width of 20 μm to 200 μm and of an arbitrary length, can penetrate through the approximately 20 nm deep ultra shallow junctions during the measurement. This can lead to false results of the μ-4*PP*

measurements. To avoid such mistakes a non-penetrating µ-4*PP* or non-damaging elastic material probe (*EM-probe*) was developed by Hillard et al [6].

4. Electrochemical micro cell

Exploring nano landscape demands high local resolution that can be determined by so-called electrochemical micro cells. The micro cell is a miniaturized form of the three electrodes conventional electrochemical cells with some special modifications to fulfill the requirements of high local resolution to investigate nano structures.

An overview of the construction of the upper frame of the micro cell is given in Fig. 1. A micro cell is simply made up of a micro capillary and object holder. The micro glass capillary is pulled and dressed planar to size and is filled with the electrolyte. In this compartment, a calomel reference and 0.5 mm thick platinum contra electrode come in contact with the electrolyte (concentrated HCl). The working electrode is the semiconductor one investigates. The three electrodes are connected with an electric source (potentiostat), which is also connected to a computer for further processing of the measured data. The positioning of the tip of the capillary on the work surface is controlled by a high resolution optical microscope. The pin diameter of the capillary varies from 2 µm to 1mm. The gasket is made up of natural silicone rubber, which hinders the leakage of the liquid at the cross sectional area of the capillary.

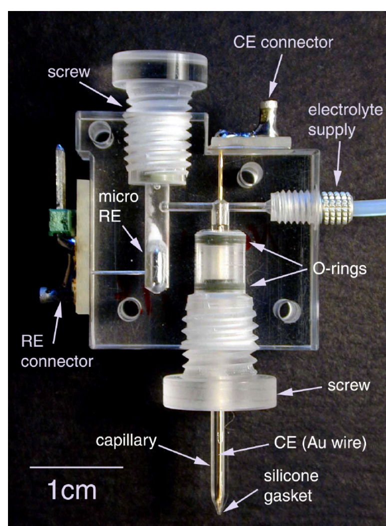

Fig. 1. Image of the upper frame of electrochemical micro cell [7].

5. The differences of macro and micro electrodes

The ohmic drop U_Ω caused by the electrolyte resistance R_Ω is equal to the resistance between the electrode surface and the equipotential surface of the Haber-Luggin capillary.

$$U_\Omega = I \cdot R_\Omega \tag{1}$$

Theoretically that means an endless macro electrode with the equipotential surface processed is parallel to the surficial area of the electrode. In that case, the electrolyte resistance R_Ω is determined by the distance between the electrode and Haber-Luggin capillary. In Eqs. (2, 3), κ is the specific electrolyte conductivity and d is the distance. Eq. (2) can be applied strictly for an electrode surface larger than 10 cm^2 [8].

$$R_\Omega = \frac{d}{\kappa \cdot A} \quad \text{for a macro electrode} \tag{2}$$

In the case of the micro electrode the equipotential surface processed between the Haber- Luggin capillary and the surface of the electrode is approximately spherical. This means the electrolyte resistance R_Ω is proportional to the reciprocal of the radius of the micro plate electrode r. Therefore Eq. (2) was modified by Newman [7] to give the required Eq. (3).

$$R_\Omega = \frac{1}{4 \cdot \kappa \cdot r} \quad \text{for a micro electrode} \tag{3}$$

Therefore the micro electrochemical cell measured currents are in the order of femto ampere (*fA*) and pico ampere (*pA*). The current resolution limit of 10 *fA* can be achieved with the following arrangements [8].

- a very good shielding of the electromagnetic perturbation field
- using a high resolution Potentiostat with low noise
- diminishing the noise using a low pass filter

In Fig. 2, a picture of the electrochemical micro cell and simplified experimental setup schemata of ultra shallow junction are demonstrated.

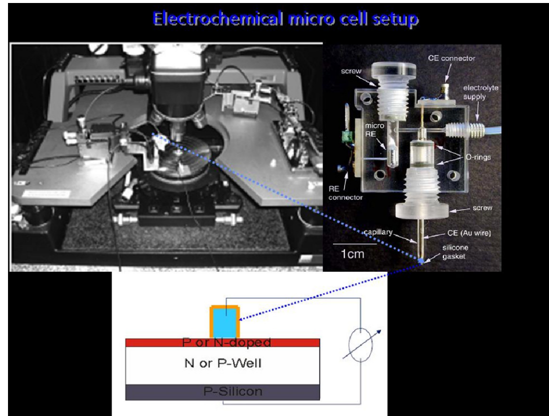

Fig. 2. Image of electrochemical micro cell and experimental setup of ultra shallow junction.

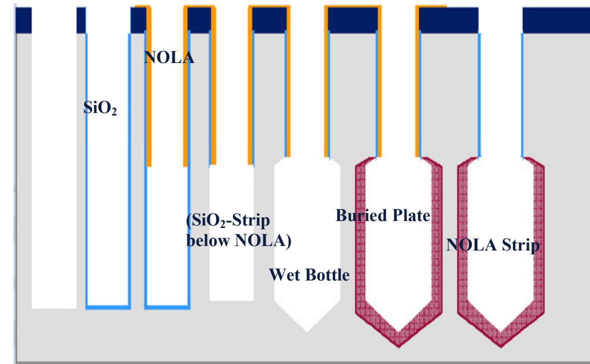

Fig. 3. Formation of the features of deep trench *DRAM*.

6. The capacity of *DT-DRAM*

To enhance the *DT-DRAM* performance; as is explained above, as well as improving the properties of the gate, some basic but decisive considerations to the capacitor should also be made. Basically, a capacitor is made up of two conductive parallel plates with a surface area A and at a distance d, which is filled with high insulator (dielectric). A capacitor is capable of storing energy as well as filtering by differentiating of low and high frequency signals in an electrical circuit. The capacitance C of a capacitor is given by

$$C \approx \frac{\varepsilon A}{d}; A \geq d^2 \quad (4)$$

where ε is the dielectric constant. Eq. (4) unambiguously clarifies that the capacitance enhancement of a capacitor's performance is proportional to the surface area, dielectric constant of the insulator and inversely proportional to the distance between the metal plates of the capacitor. This matter of fact requires that the bail shaped capacitor of the status quo to be substituted by the *DT*-capacitor for the sake of the aspect ratio. Recalling that the capacitance of the capacitor measures the amount of charges Q stored on each plate for a given potential difference V, it is therefore necessary to implement a metrology method, which characterizes the properties of *DT*-capacitor precisely.

The evolutions of deep trench capacitor (*DT-DRAM*) features are highlighted in Fig. 3. These feature extensions of the deep trench capacitors from the cylindrical shape to bottle shape are designed to enhance the capacitor performance by 25% due to improvement of the aspect ratio [10]. The main issue of this feasibility study is to focus on the electrochemical characterization of every possible area of the capacitor features presented in Fig. 3; starting from the cylindrical up to the bottle shaped capacitor of the *DT-DRAM*. The manufacturing process of such deep trench based capacitors is discussed in [10].

7. Physical quantities obtained from electrochemical measurements

With a combination of the micro electrochemical cell, a good potentiostat and using some electrochemical methods such as cyclic voltammetry and impedance spectroscopy, one can obtain a lot of information that can easily be interpreted to characterize the electrochemical reactions that take place on the interface of a work electrode. Measuring with a potentiostat means a potential controlled measurement and the response will be the current I or if it is normalized to the surface the current density i. From the current density the charge Q, capacity C and sheet resistance R can be obtained. From these physical quantities one obtained the layer thickness, layer resistance, the roughness, the dielectric constant, the thickness of space charge, surface area and doping concentration [6]. In potentiodynamic methods, the potential increases with time, when oxidation at the anode electrode takes place and vice versa, when reduction at the cathode electrode occurs. The current density i will be plotted versus the desired potential range (Fig. 4). The charges versus potential can be plotted by a

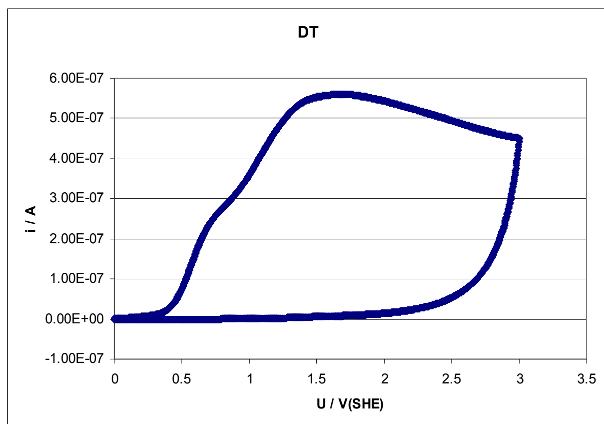

Fig. 4. Typical cyclic voltammogramme of SiO_2 of deep trench *DRAM.*

numerical integration of the measured current. Potentiodynamic methods also enable a simultaneous measurement of a one frequency capacity with the lock-in-amplifier parallel to a cyclic voltammetry measurement [6]. The surface area of the specimen can be converted by calculating the ratio of the well known oxide layer growth current density 100 μA/cm^2 [11], derived from the high field mechanism law of SiO_2 and the amount of current which fluxed during the experiment of cyclic voltammetry, which could be obtained from such cyclic voltammogramme depicted in Fig. 4.

The last but not the least versatile electrochemical characterization method to characterize the intrinsic electrical properties and the interface of any material is impedance spectroscopy. The principle of impedance Spectroscopy is the analysis of the impedance (resistance of alternating current) of the observed system with subject to the applied frequency and exciting signal. This analysis provides quantitative information about the conductance, the dielectric coefficient, the static properties of the interfaces of a system, and its dynamic change due to adsorption or charge transfer phenomenon. Impedance spectroscopy uses alternating current with low amplitude. This facilitates a non-invasive observation of any sample without any or less influence on the electrochemical state.

The electrical impedance of an electrochemical cell can be measured either directly with an impedance analyzer or with a combination of a frequency response analyzer and an electrochemical interface unit. The electrochemical interface is a high bandwidth Potentiostat which provides the dc bias voltage or current, and a small sinusoidal ac signal (typically a few mV) from the frequency response analyzer is superimposed. The ac response from the cell over a range of applied frequencies is analyzed by the frequency response analyzer and the impedance is calculated [12].

Data collection, display and analysis are normally controlled by software running on a personal computer. Equivalent circuit modeling has been accepted as the means of interpreting electrochemical impedance results [13], as this offers a convenient way of analyzing and investigating changes in cell behavior. Other publications describe the theory, experimental practice and interpretation in more detail [14-18]. Results are plotted in the complex plane (Nyquist plot: Fig. 5(a)) or as magnitude and phase versus frequency (Bode plot: Fig. 5(b)). Hereby are the ultra shallow junction XP: P-doped on N-well on P-substrate and XN: N-doped on P-well on P-substrate.

Furthermore the capacity *C* of *USJ* can be calculated from the data of the imaginary impedance *Z*'' at a single

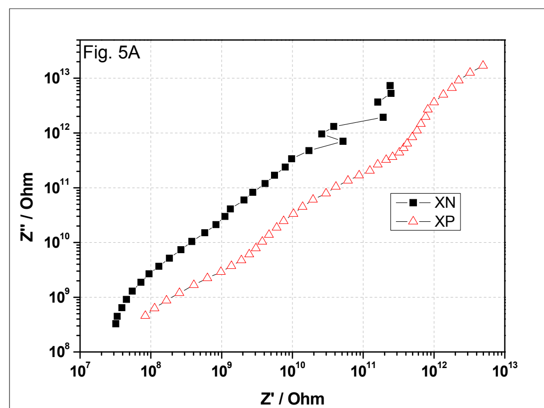

(a)

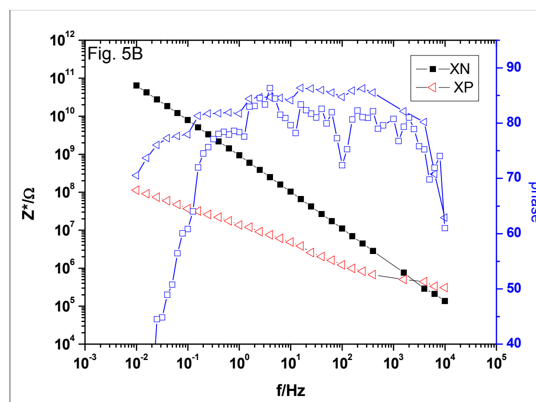

(b)

Fig. 5. Demonstrated are the (a) Nyquist and (b) Bode plot.

frequency f using;

$$C=1/2f\pi Z'' \qquad (5)$$

Now the doping concentration of the semiconductor can be obtained using the data from capacity C and applied potential, utilizing the Mott-Schottky Eq. (6) [20]. Thus the doping concentration can be obtained from the slope of a line by plotting C^{-2} versus the applied potential E, which is imposed to measure the impedance of a semiconductor. Hereby the flat band potential E_{FB} can be obtained by extrapolating the linear slope towards E-axis of abscissa. From the direction and form of the linear slope, one can get the information of doping type (n or p doing) and doping concentration.

$$\frac{1}{C_{SC}^2} = \frac{2}{e_0\varepsilon\varepsilon_0 N_D}\left[E - E_{FB} - \frac{KT}{e}\right] \qquad (6)$$

III. EXPRIMENTAL

The cyclovoltammetry (*CV*) and electrochemical impedance spectroscopy (*EIS*) measurements were done at Fraunhofer-IKTS Dresden. The electrochemical micro cell was connected to an Autolab PGStat30 Potentiostat from Metrohm and for further data processing to a computer [19]. The *EIS* measurements were carried out with perturbation amplitude of ±10 mV in a frequency range from 100 KHz to 10 mHz. For equivalent circuit calculations and curve fitting *EIS*-Spectrum analyzer software and Origin 7.5 were used respectively. A polarization microscope assisted the targeting of the work position of the micro capillary on the wafer. To avoid sample damage the pressure of the capillary on the specimen was controlled by a mechanical motor. The micro capillary with an opening diameter of 50 µm surrounded by a silicone gasket included the counter electrode made of tiny platinum wire and an Ag/AgCl reference electrode (207 mV at 25 °C) [11]. The micro cell is filled with an acetate buffer (pH = 6) electrolyte.

1. Description of specimen

P1= P-doped on N-well on P-substrate (not annealed)

P2 = P-doped on N-well on P-substrate (annealed)

P3= N-doped on P-well on P-substrate (not annealed)

P4= N-doped on P-well on P-substrate (annealed)

P5 = P-doped on P-substrate (annealed)

P6= P-doped on P-substrate (a double doping concentration & annealed)

P7= N-doped on P-substrate (annealed)

P8= N-doped on P-substrate (a double doping concentration & annealed)

P9= P-well on P-substrate (annealed)

P10= N-well on P-substrate (annealed)

2. Experimental results

The results of the electrochemical impedance spectroscopy and cyclic voltammetry measurements of *USJ* are presented in Fig. 6 to Fig. 13. The results obtained clarify qualitatively the influence of doping concentration, doping profile, doping type (*N* or *P* doping) and the well influence of the *USJ*.

In Fig. 6 is a result of EIS of the specimen P1 to P4 in the form of a Nyquestplot presented. Hereby the doping type (*P* or *N* doping) and doping activation state (annealed or no annealed) could be distinguished.

Furthermore differences of impedance due to the influence of annealing, the influence of doping concentration and the influence of the presence of any type of a well (whether n-well or p-well) could be demonstrated at Fig. 7, Fig. 8 and Fig. 9 respectively. The specimens not annealed without consideration of the doping type showed larger impedance than the annealed

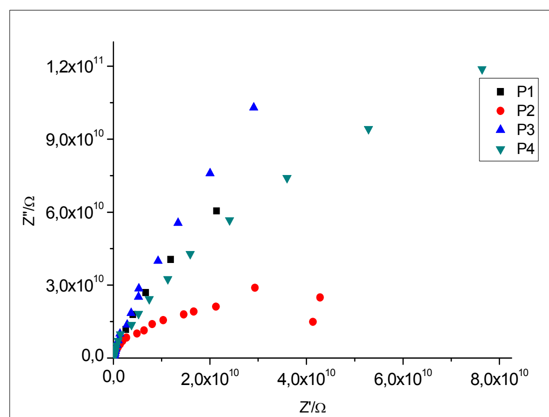

Fig. 6. Impedance spectra of the specimens P1 to P4.

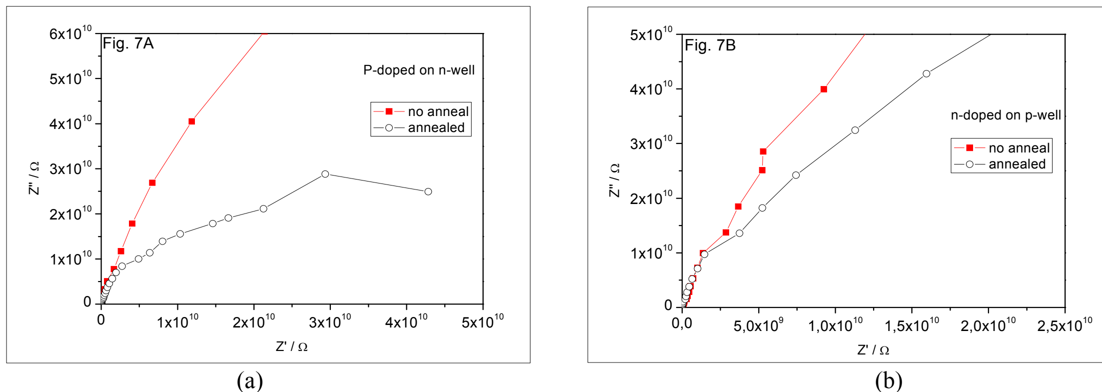

(a) (b)

Fig. 7. Influence of annealing (a) p-doped on n-well (b) n-doped on p-well.

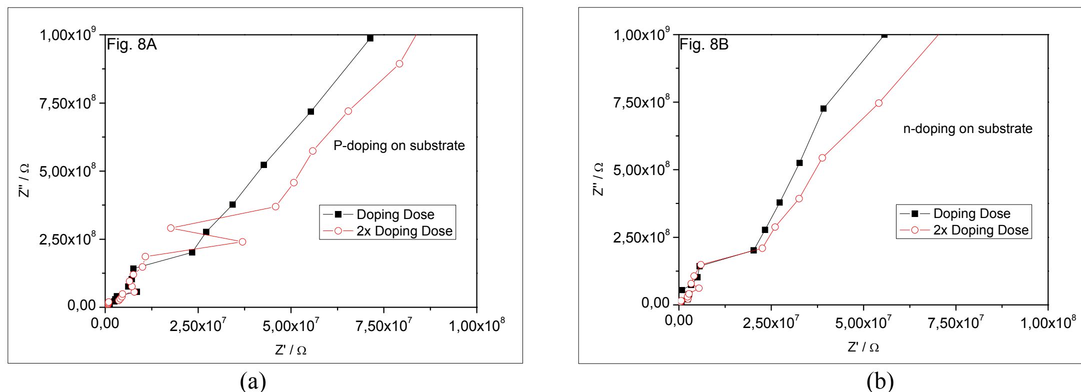

(a) (b)

Fig. 8. Influence of the doping concentration on the substrate (a) P-doping on substrate (b) n-doping on substarte.

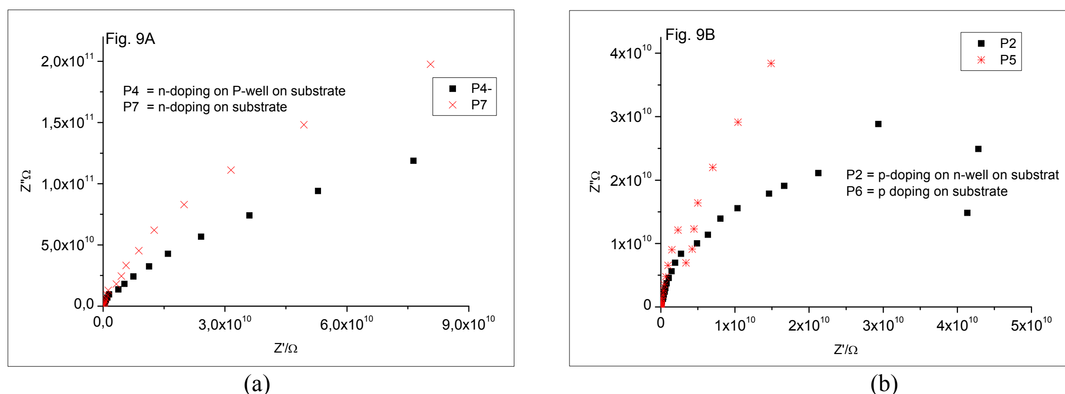

(a) (b)

Fig. 9. Influence of the well type of the specimens (a) P4 and P7 (b) P2 and P5.

specimens. Hereby, during annealing, the healing of the defect and activation of the semiconductor structure takes place. Therefore the annealed specimens show less impedance value compared to the specimens that were not annealed. The Specimens with double doping concentration (ca. 10^{36} doping atoms) have less impedance than the specimens which are simply doped (ca. 10^{18} doping atoms). This matter of fact comes due to increase of the conductivity of the semiconductor material with increasing doping concentration.

In Fig. 10 are the cyclic voltammogrammes of the specimens P1 to P4 presented. The results demonstrate the increase of the oxidation peak of the annealed n-doped specimen P4 compared to the not annealed n-doped specimen P3. On the contrary the oxidation peak of the annealed p-doped specimen P2 decreases in comparison to the not annealed p-doped specimen P1, which is vice versa to the former one.

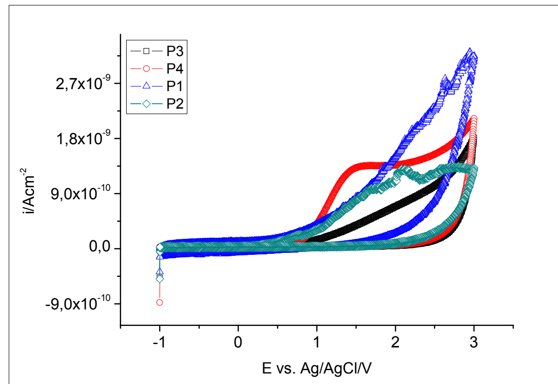

Fig. 10. Cyclic voltammogrammes of the specimen P1to P4.

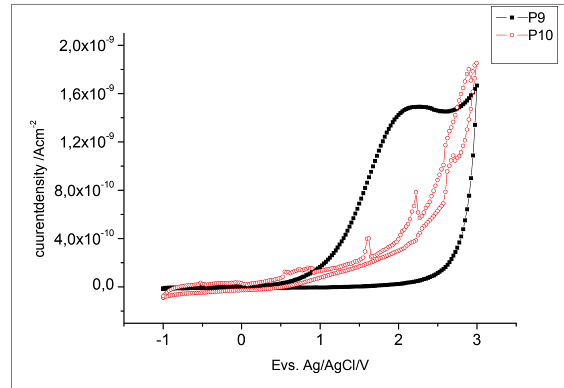

Fig. 12. Cyclic voltammogrammes of the specimen P9 and P10.

Hereby it is observed that the influence of the well type (n-well or p-well) plays a bigger role than that in the annealing process (doping activation) on the oxidation process of the specimen.

In Fig. 11 are the cyclic voltammogrammes of the specimens P5 to P8 presented. Hereby all specimens are annealed but with differences in doping type and doping concentration. Despite the differences in doping type and doping concentration all specimens showed the same oxidation peak form as if the double doping concentration of the specimen plays no role. This result shows the contrary of the results obtained from the impedance spectroscopy. The calculated charge concentrations, which were obtained by integration of the inner space of the cyclic voltammogramme, show a slight difference.

In Fig. 12 are cyclic voltammogrammes of the specimen P9 and P10 presented. Specimen P9 (P-well on P-substrate) and Specimen P10 (N-well on P-substrate) are both annealed and with P-substrate. The results demonstrate the influence of the well type clearly. The shape of the cyclic voltammogramme and the oxidation peak of specimen P10 are narrower and higher than of the specimen P9 respectively. Hereby the slightly higher oxidation peak resulted from the annealing process; only the result of the shape of the cyclic voltammogramme is likely to be interpreted as the influence, which outcomes from the well type of the specimen.

The charge concentrations of the specimens can be calculated by integration the inner space of their cyclic voltammogrammes. From the plot of the charge concentration versus the applied potential, the capacity of the specimens can be calculated. Hence the capacity and the reactive area of the specimen are known; the layer thickness of the ultra shallow junctions can be estimated.

A plot of the charge concentration versus the applied potential of the specimen P1 to P4 is presented in Fig. 13. The result demonstrates an enhancement of the charge

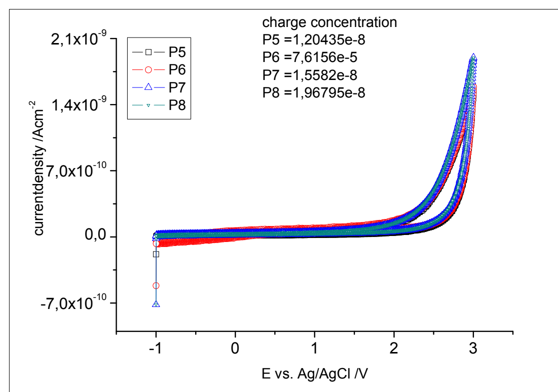

Fig. 11. Cyclic voltammogrammes of the specimens P5 to P8.

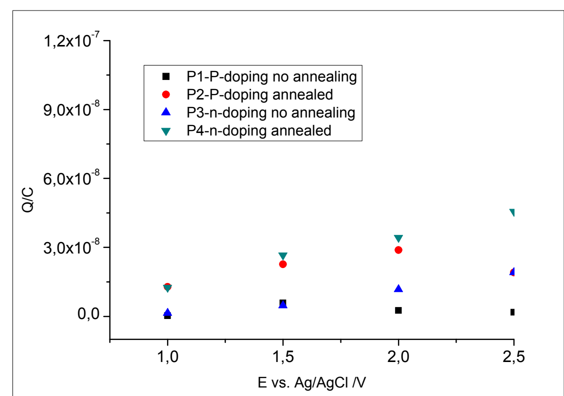

Fig. 13. Charge concentration vs. applied potential.

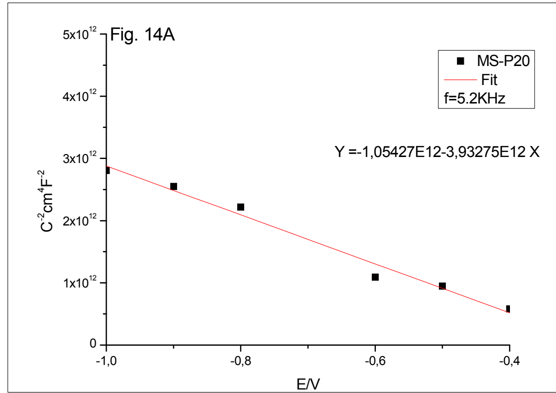

(a)

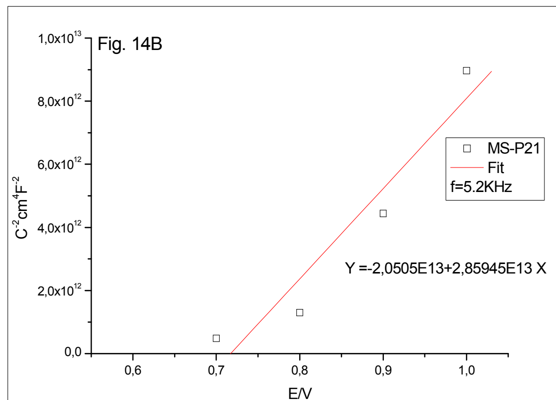

(b)

Fig. 14. Mott-Schottky (*MS*) Plots of the specimen (a) P9 and (b) P10.

concentration of the specimens' according to the applied potential. The obtained charge concentration enhancement of the specimens is as follows: P4>P2>P3>P1.

As an example Mott-Schottky (*MS*) plots of ultra shallow junction's of the specimens P9 and P10 are presented in fig. 14. These are obtained from the result of the imaginary impedance data by calculating the capacity (C =1/2fπZ'') at a single frequency of 5.2 kHz. These results clarify qualitatively and quantitatively the influence of doping concentration, doping profile, partially doping type (N or P dopings) and the well influence on USJ.

Furthermore the doping concentrations N_D/cm^3 were calculated from the slope of Mott-Schottky (*MS*) plots ($1/C^2$ versus applied potentials V) considering the linear slope of the Mott-Schottky (*MS*) Eq. (7) [19] and are depicted on Table 1.

$$N_D = \frac{2}{\varepsilon_{Si}\varepsilon_0 e_0 m} \quad (7)$$

Table 1. Doping concentration of the specimen 1P to P10

specimen	doping concentration N_D/cm^3
P1	8.6964e19
P2	4.1419e19
P3	7.6950e19
P4	4.4032e19
P5	4.6694e19
P6	9.1429e19
P7	3.9928e19
P8	1.0768e20
P9	2.9874e18
P10	4.1113e17

Hereby are:

ε_{Si} = 12.1

ε_0 = 8.8542e-12 F/m

$\mathbf{e_0}$ = 1.60218e-19 C

m = linear slope mx +y = 0

3. The results of doping concentration

- The results of the doping concentration calculated as mentioned above were as expected.
- The results of the Mott–Schottky Plots of the specimens P5 to P6 and P7 to P8 depict as expected an increasing doping concentration respectively.
- The doping concentration of the specimens P1 to P2 and P3 to P4 is reduced through the annealing process of the specimen.
- The doping concentrations of the not annealed n-doped and p-doping specimens are the same. The linear slope of the N-doped specimen P3 and P4 were not as expected.

IV. CONCLUSIONS

In summary, a feasible study of electrochemical methods in combination with electrochemical micro cells to characterize nano semiconductor structures of *DT-DRAM* was discussed. Metrology methods to characterize semiconductor structures at various technological nodes are discussed, attempting to depict the strengths and weaknesses of electrochemical methods compared to other existing methods. It is shown how precise electrochemical methods respond to many unsolved metrological problems in the semiconductor industry. From this point of view there is an opportunity in the

future for electrochemical methods to be implemented as Inline analysis techniques.

ACKNOWLEDGMENTS

Thanks to Dr. Michael Schneider from the Fraunhofer-IKTS and Dr. C. Ehlers from Qimonda Dresden for their kind advice and sophisticated discussion.

This joint venture project was financially supported by the Federal Ministry of Education and Research of the Federal Republic of Germany (BMBF) and Qimonda Dresden (Project No 13 N 9432).

REFERENCES

[1] ITRS/2007_*Chapters/2007*_Metrology.pdf , 2007.
[2] R. Pelt, Altera Corporation San Jose California, USA, 2007.
[3] I. Eisele, *Tutorial*, federal army University Munich, 2007.
[4] P. Weidner, A. Kasic, T. Hingst and T. Lindner: *Semiconductor FABTECH- 32nd Edition*, Qimonda.
[5] M. Gostein, J. Byrnes, A. Mazurenko and T. Bonanno, Advanced Metrology Systems Qimonda.
[6] R. J. Hillard, R. G. Mazur*, Mat. Res. Soc. Symp.* Vol.810, 2004.
[7] A. Moehring: *PhD. Thesis*, Heinrich-Heine University Duesseldorf/Germany 2004.
[8] T. A. Suter, *PhD. Thesis*, Eidegen, Techn. Hochschule Zuerick
[9] J. Newman, *J. Electrochem. Soc.* 113 501-502 , 1966.
[10] J. Amon et al, *Report*, Infineon technologies Ag
[11] S. Schroth, *diploma thesis*, technical university of Dresden 2007
[12] T-C. Lo, *Tutorial*, Department of Electrical and Electronic Engineering, the Hong Kong University of Science and Technology, 1996.
[13] J. R. Macdonald, *J. Electroanal. Chem*. 307, 1991.
[14] J. Maier, *Festkoerper Fehler und Funktion*, Teubner Studienbuecher Leipzig, 2000.
[15] F. B. Mansfeld, *Tech. Report 026, Solartron*, Farnborough, UK, 1991.
[16] B. A. Boukamp, *Equivalent Circuit, University Twente*, Report CT89/214/128, The Netherlands, 1989.
[17] F. B. Mansfeld, H. Shih, and C. H. Tsai, *Computer Modeling in Corrosion*, ASTM STP 1154, 1992.
[18] F. Mansfeld, H. Shih, H. Greene and C. H. Tsai, "Analysis of EIS Data for Common Corrosion Processes ASTM," STP 1188, 1993.
[19] P. Schmuki, *J. Electrochern. Soc.*, Vol.142, 1995.

Tadios Tesfu Zeru received Diploma from the Department of Chemistry in 1999, University of Kassel/ Germany and Ph.D. from the Department of Physical Chemistry, the University of Justus Liebig Giessen/Germany, in 2004. From 1997–1999 he worked as scientific assistant at Max-Planck Institute of Stuttgart, from 1999 – 2004 scientific coworker in the University of Justus Liebig in Giessen, and in 2005 as a lecturer and a supervisor in the laboratory of Inorganic and Physical Chemistry of Technical University of Darmstadt /Germany. From 2006 to 2008 postdoctoral in Leibniz Institute of Polymer Researches (IPF) and the Fraunhofer Center of Nanoelectronic Technologies (CNT) in Dresden and since 2009 scientist in the field of corrosion and sustainable energy techniques at KWI-Dechema in Frankfurt/Germany.

Stephan Schroth received diploma in 2007 and Ph.D. in 2011 at the Department of Physics from the Technical University of Dresden. From 2006 to 2011 he was scientific coworker at Fraunhofer-IKTS in Dresden and since 2011 R&D lead engineer for Medical Devices in Pforzheim/Germany.

Peter Kuecher, is a Director of the Fraunhofer-CNT (Center of Nano-electronic Technologies) in Dresden since 2005. Prior to this assignment he was President of Infineon Flash and till end of 2002 Managing Director of Infineon SC300, former SEMICONDUCTOR300 - the world's first 300mm line. For his engagement in 300mm he received the European Semiconductor Award in 2000. From 1993 – 1996 he was the Siemens project manager in the joint project with IBM and Toshiba in East Fishkill, NY to develop 0.25 um technology based on a 256M DRAM . Prof. Kuecher held various positions in process development with Siemens Corporate Research and managed several European projects within ESPRIT and JESSI. His Ph.D. is in Applied Physics from the University Regensburg, Germany. In August 2006 Dr. Kuecher was appointed to honorary professorship in the specified field of microelectronics at Technical University Dresden, Germany.